Aluminum-Based Engineered Plasmonic Nanostructures for the Enhanced Refractive Index and Thickness Sensing in Ultraviolet-Visible-Near Infrared Spectral Range

Pankaj Arora[*] and Harsh V. Awasthi

Abstract—We engineer Aluminum (Al) based periodic plasmonic nanostructures for enhanced refractive index and thickness sensing, which offer to access complete ultraviolet-visible-near infrared spectral range for surface plasmon resonance sensors. Al-based periodic nanostructures on top of a thin homogeneous Al metal coated on a BK-7 glass substrate were designed by systematic variation of geometrical parameters using Rigorous Coupled Wave Analysis and finite elements full wave solver. The shift in surface plasmon mode excited on the nanostructure-analyte interface was used to measure the variation in refractive index, and the number of waveguide modes with the increase in the thickness of the analyte was used to capture the variation in thickness of the analyte. The proposed nanostructures of period 400 nm and an aspect ratio of 0.1 offered a sensitivity of 400 nm/RIU and full width at half maximum of 18 nm resulting in a figure of merit of 22. These Al-based plasmonic nanostructures have potential to be used as refractive index and thickness sensor due to a high figure of merit, high localization of the field, and very low aspect ratio that is needed to maintain laminar flow of analyte.

1. INTRODUCTION

Estimation of refractive index and thickness of analytes is a major key to identifying changes to a surface and possible implications of those changes. Plasmonic nanostructure-based Surface Plasmon Resonance (SPR) sensors have attracted tremendous attention due to the strong enhancement and high confinement of field at sub-wavelength scale, the possibility of Surface Plasmon (SP) excitation at normal incidence and provide a method to integrate plasmonic devices on a planar chip [1–7]. Though nanostructure-based plasmonic sensors have many advantages, improving their performance is still an important issue.

Noble metals such as gold and silver are mostly used plasmonic metals for majority of the plasmonic sensors. However, these noble metals have inherent limitations hindering the development of plasmonic devices towards the blue and ultraviolet parts of the spectrum due to strong interband transitions [8]. The use of Aluminum (Al) in plasmonic nanostructures, which is relatively economical, widely available, and compatible with optoelectronics devices, offers new possibilities to access the complete UltraViolet-Visible-Infrared (UV-Vis-IR) spectral range [9–11]. Recently Al has been widely used in the applications of plasmonic such as biosensors, photodetection, surface-enhanced Raman scattering, and surface enhanced fluorescence [12–15].

To improve the sensing performance of SPR sensor, refractive index sensors based on Fano resonance [16], topological insulator film [17], and multilayer structures [18] have been reported in the recent past, which offer a very good sensitivity, broad measurement range, and high figure of merit due to deep subwavelength confinement of light in plasmonic waveguide, the requirement of small incident

angle on topological films, and EIT like spectral splitting in multilayer structures respectively. But the requirement of sub 10-nanometer feature size and bulky Kretschmann configuration arrangement to excite SPs is still a major issue.

In this paper, we extend the studies of plasmonic nanostructure-based sensors and engineer very low aspect ratio Al-based plasmonic nanostructures under normal incidence condition with Transverse Magnetic (TM) polarization of light for their sensitivity to an analyte (acting as a superstrate) with different refractive indices and thicknesses. A major advantage of our proposed nanostructure is the normal incidence excitation of SPs which does not need any bulky and complicated Kretschmann configuration arrangement for phase matching condition. Moreover, the proposed plasmonic nanostructures have been engineered with a very low aspect ratio, while taking into account the fabrication constraints. The transmittivity amplitude, the width of SPR curve, and the sensitivity are considered the main aspects while engineering the geometrical parameters of periodic nanostructures using Rigorous Coupled Wave Analysis (RCWA) [19]. The shift in SP excitation is used to measure the changes in the refractive index of the analyte, and the number of excited higher order waveguide modes is utilized to capture the variation in the thickness of analyte by accessing the complete UV-Vis-near IR spectral regime. The proposed nanostructures offer the improvement by a factor of 4 in the Figure of Merit (FOM) as compared to sensors with gold based plasmonic nanostructures [20]. For normal incidence, since the resonance wavelength is found to be almost close to the period of the nanostructure, the ± 1 diffraction orders are responsible to excite SPs in the engineered nanostructures, and nanostructure of period $400\,\text{nm}$ offers a sensitivity of $400\,\text{nm/RIU}$. A longer period is found to be a higher refractive index sensitivity; however, a short period is preferred for a short decay length [21].

Such structures can be easily fabricated using conventional semiconductor processing techniques involving electron beam lithography, a metal evaporation step followed by a lift-off process. In these structures, for refractive index and thickness estimation of an analyte, an experiment involving shining a TM polarized broadband light from the top normal to the surface and collection of the transmitted light from the bottom of the substrate using a high numerical aperture objective can be easily performed [4, 22].

2. RESULTS AND DISCUSSION

The schematic of the proposed plasmonic nanostructures is shown in Fig. 1(a). The substrate for the structures is assumed to be BK-7 glass with a refractive index of 1.542. The metal considered in all our
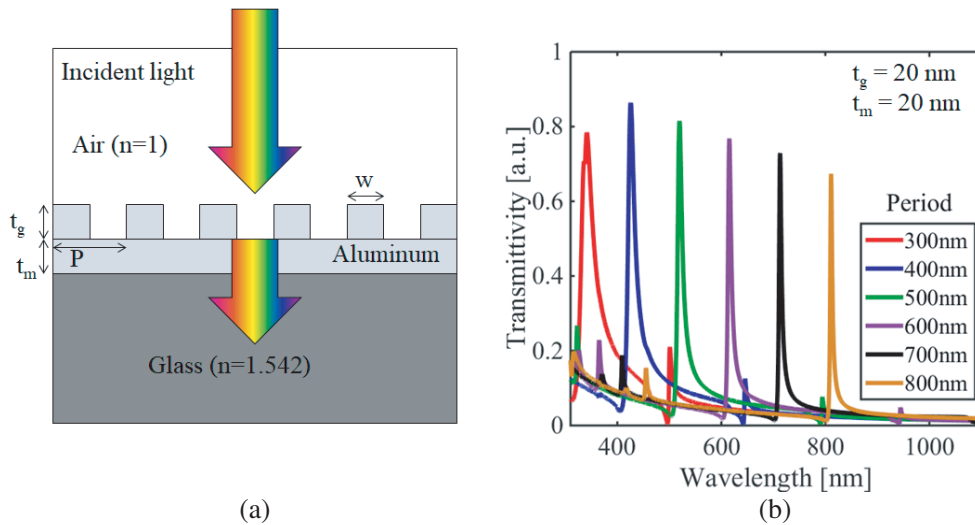

(a)   (b)

Figure 1. (a) Schematic diagram (not to scale) of the proposed Al-based periodic plasmonic nanostructure. (b) Transmittivity spectra for proposed nanostructure with variation in the period (P) for $t_g = 20\,\text{nm}$, and $t_m = 20\,\text{nm}$.

simulations is Aluminum (Al) with a permittivity defined by the Drude's model as given in Equation (1), and the parameters were obtained from [23, 24].

$$\varepsilon_m(\lambda) = 1 - \left(\frac{\lambda^2 \lambda_c}{\lambda_p^2 (\lambda_c + j\lambda)} \right) \tag{1}$$

where $\lambda_p = 1.0657e^{-7}$ m and $\lambda_c = 2.4511e^{-5}$ m denote the plasma wavelength and collision wavelength, respectively.

In the proposed structures, a homogeneous thin metal layer of Al was considered between the glass substrate and periodic plasmonic nanostructures, to convert the signature of SPs as transmission peaks instead of transmission dips. The transmission peaks occur since under most conditions almost all of the coming light is reflected back from the top (since metal acts like a mirror) except for momentum matching condition for different resonances wherein SP modes are excited at the nanostructure-analyte interface. When SPs are excited on the nanostructure-analyte interface, due to the very small thickness of the homogeneous Al metal ($t_m = 20$ nm), a radiative decay of SP occurs through the glass substrate, and the light leaks through the substrate at specific angles depending on refractive indices of substrate and superstrate [25]. Such radiative decay of SP modes has been used in our recent work in leakage radiation microscopy-based experiments [20, 22].

The broadband simulations were performed for normal incidence from the top of the structures using a homemade RCWA program, and the field distributions were obtained using a commercial finite elements full wave solver (Comsol Multiphysics). The geometrical parameters of the proposed structures namely the period 'P', the thickness of homogeneous metal layer 't_m' and the thickness of periodic nanostructures 't_g' were changed systematically, and the transmittivity was measured from the bottom of the substrate for TM polarization for a range of wavelengths from UV to near IR regime. The final geometrical parameters were chosen during the simulations to achieve the narrowest line width of the SPR curve and high signal contrast and sensitivity. Fig. 1(b) shows the transmittivity spectra for Al-based plasmonic nanostructures with $t_m = t_g = 20$ nm, where the SP resonance wavelength was easily tuned in complete UV-VIS-IR regime by changing the period of nanostructures.

Figure 2(a) shows the transmittivity spectra for t_g of 20 nm and P of 400 nm with different thicknesses of metal height (t_m). As t_m was increased towards 30 nm, the maximum transmittivity value was reduced up to 0.5 (green color) due to absorption of Al metal preventing a lot of light, resulting in low signal contrast but with narrowest Full Width at Half maximum (FWHM). When t_m was lower than 20 nm (red color), the transmittivity value was found higher but with higher FWHM since due to a very thin layer of Al metal; most of the light was directly transmitted to the substrate; the interaction of field due to SP excitation on top of nanostructure was less which resulted in increased FWHM. As mentioned, since most of the light got transmitted to the substrate due to the very thin Al
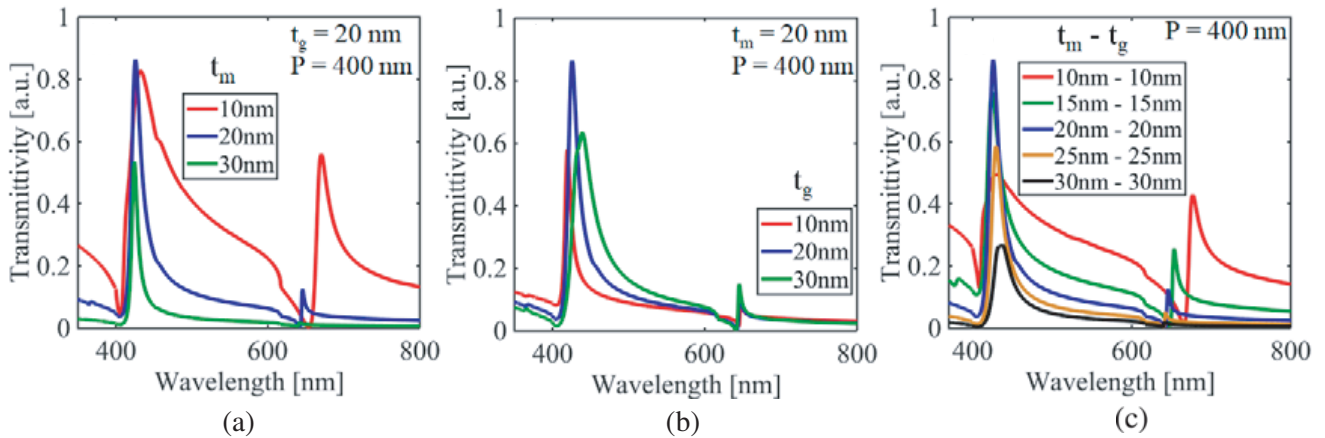

Figure 2. Calculated transmittivity spectra as a function of wavelength for plasmonic nanostructures of period (P) = 400 nm with (a) variation in the thickness of metal (t_m), (b) variation in nanostructure height (t_g), (c) variation in both metal height and nanostructure height ($t_m - t_g$) respectively.

layer, the interaction of field due to substrate mode on thin meta-substrate interface was more, and as a result, the second peak of transmittivity around ($\lambda = 650$ nm) was higher for $t_m = 10$ nm than other cases. Hence, a careful choice of the thickness of the thin metal (t_m) of 20 nm (blue color) resulted in a decent value of signal contrast and FWHM.

Figure 2(b) shows the transmittivity spectra for t_m of 20 nm and P of 400 nm with different heights of periodic nanostructures (t_g). It was noticed that the value of 20 nm (blue color) for t_g resulted in a high signal contrast and narrow FWHM.

Figure 2(c) shows the transmittivity spectra for P of 400 nm with different thin metal heights (t_m) and nanostructure heights (t_g) together. A set of values $t_m = t_g = 20$ nm was found to be the optimal value for the proposed structures, which results in a high signal contrast and lowest FWHM value.

Therefore, from Fig. 2, it is observed that metal height (t_m) of 20 nm and nanostructure height (t_g) of 20 nm exhibit an optimum compromise between high signal contrast and narrow FWHM for SP resonance.

After optimizing the geometrical parameters of plasmonic nanostructures, an analyte (acting as a superstrate) of thickness $t_a = 250$ nm with a refractive index of $n_a = 1.33$ was assumed on top of the proposed structures as shown in inset (i) of Fig. 3(a). It was observed that for a t_a of 250 nm, P of 400 nm, $t_m = t_g = 20$ nm, and for an analyte refractive index of 1.33, the structures exhibited three distinct transmission peaks at 420 nm, 560 nm, and 650 nm as shown in the blue curve of Fig. 3(a). The electric field (E_z) distributions for this geometry with analyte refractive index of 1.33, at wavelengths 420 nm, 560 nm, and 650 nm are shown in Figs. 3(b)–(d), respectively.
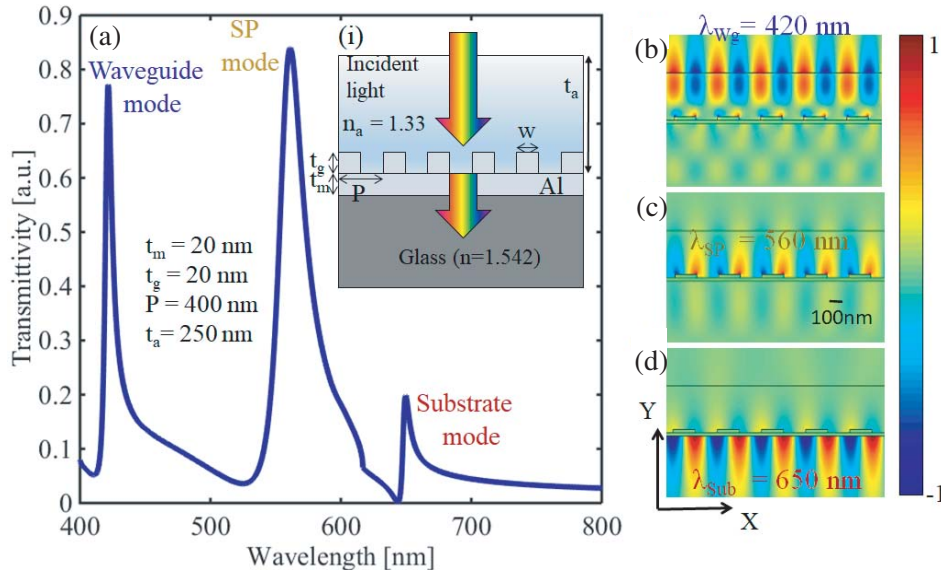

Figure 3. (a) Transmission spectrum for the plasmonic nanostructures of period (P) $= 400$ nm, $t_g = t_m = 20$ nm, $n_a = 1.33$ and $t_a = 250$ nm; Inset (i) represents schematic diagram (not to scale) of the proposed Al-based periodic plasmonic nanostructure with an analyte of refractive index (n_a) and thickness (t_a); Electric field (E_z) distribution for (b) waveguide mode, (c) SP mode, and (d) substrate mode respectively.

It was observed that the resonant peak in transmission at a wavelength of 420 nm is due to a dielectric mode which resembles a conventional waveguide mode as shown in Fig. 3(b). Since most of the field propagates away from the metal-dielectric (analyte) interface, resulting in lower propagation losses due to weaker interaction with the metal and resembles a conventional waveguide mode, we named it as a dielectric waveguide mode. The resonance at 560 nm is attributed to the fundamental SP mode at the plasmonic nanostructures and analyte interface (Fig. 3(c)). The electric field distribution for this SP mode shows a strongly confined mode at the nanostructure-analyte interface. The third resonance at 650 nm is due to excitation of the surface plasmon at thin homogeneous Al metal and glass

substrate interface as shown in Fig. 3(d). It should also be noted that the transmittivity corresponding to the substrate mode (Fig. 3(d)) at 650 nm is significantly reduced due to the absorption of the thin homogeneous Al metal layer.

To utilize these plasmonic nanostructures as a refractive index sensor, the refractive index of the analyte (n_a) was varied by 0.01 RIU, and transmission characteristics for plasmonic nanostructures of $P = 400$ nm, $t_m = t_g = 20$ nm, and $t_a = 250$ nm, were calculated as shown in Fig. 4(a). The right shift in the resonance peak corresponding to SP excitation at the nanostructure-analyte interface, with the increase in the analyte's refractive index, was observed as shown in Figs. 4(a) and (b) as green and red curves, respectively. The SP resonance wavelength for 1D plasmonic nanostructures under normal incidence condition can be explained as follows:

$$\lambda_{SPR}(n, i) = \frac{P}{i}\left(\pm\mathrm{Re}\left(\frac{\varepsilon_m n_a^2}{\varepsilon_m + n_a^2}\right)^{1/2}\right) \tag{2}$$

where P is the period of the nanostructure, i the diffraction order, ε_m the dielectric constant of the metal, and n_a the analyte refractive index [21]. From Equation (2), the resonance wavelength is close to $P \times n_a$, only if the first order diffraction order is present. In other words, the refractive index sensitivity is mainly determined by the periodicity of the nanostructures, that is sensitivity $= \Delta\lambda_{SPR}/\Delta n_a \approx P$. The FWHM for the SP resonance peak was extracted as 18 nm, and the sensitivity of this mode to a change in
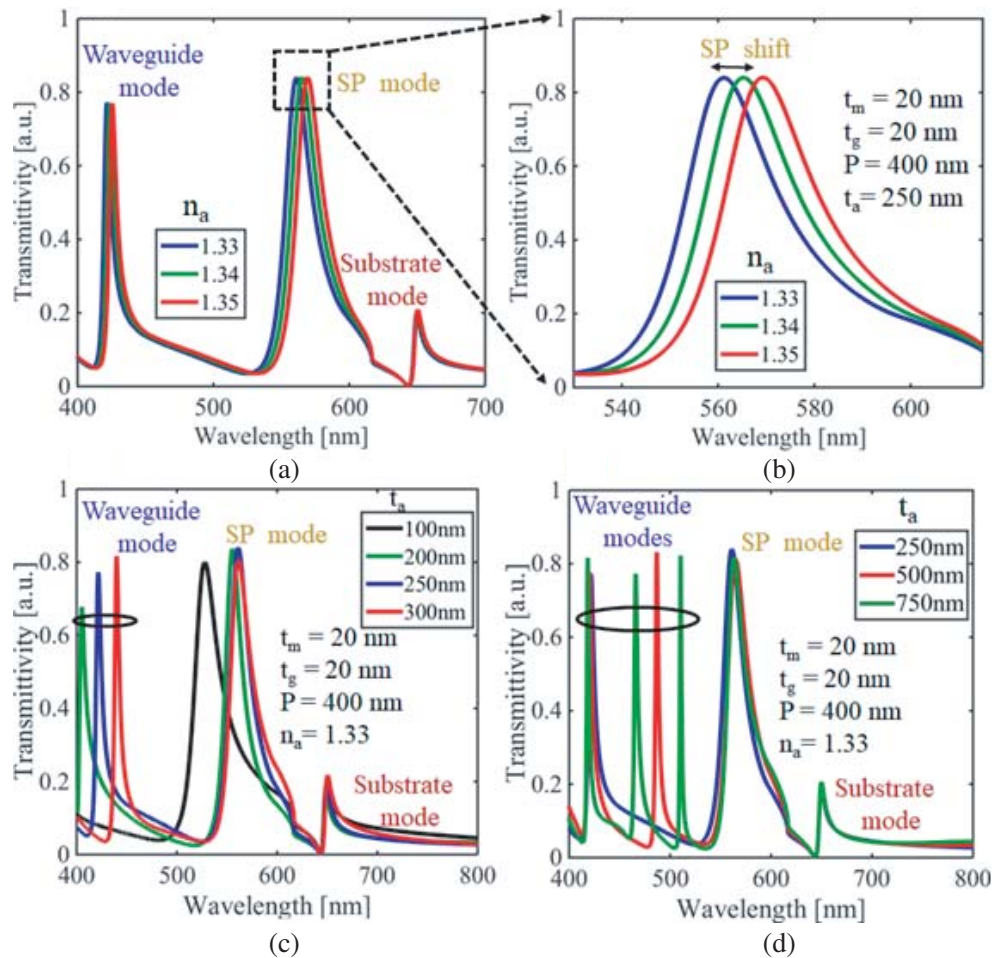

Figure 4. Transmission spectrum for the proposed plasmonic nanostructures of the period $(P) = 400$ nm, $t_m = t_g = 20$ nm and with (a) variation in the refractive index of the analyte (n_a), (b) zoomed in region corresponding to SP mode (c)–(d) variation in the thickness of the analyte (t_a) respectively.

refractive index was $400\,\text{nm/RIU}$ for $P = 400\,\text{nm}$. This resulted in a FOM of 22 which is an improvement by a factor of 4 as compared to SPR sensors with gold based plasmonic nanostructures [20, 22]. A longer period had a higher refractive index sensitivity; however, a short period is preferred for a short decay length. A possible way to balance the trade-off between the high refractive index sensitivity and short decay length is the use of oblique incident light on a longer period for higher sensitivity, which results in small SP resonance wavelength and shorter decay length.

Next, we simulated the transmission characteristics for the structures with the same parameters as used in Figs. 4(a) and (b) but with the variation in the thickness of the analyte (t_a). Figs. 4(c) and (d) show the transmittivity spectra for the structure of $P = 400\,\text{nm}$, $t_m = t_g = 20\,\text{nm}$, $n_a = 1.33$ with varying the thicknesses of the analyte. In Fig. 4(c), a shift in the SP mode was noticed with the variation in the thickness of the analyte, but after a thickness of $t_a = 250\,\text{nm}$, the SP mode was found to be independent of the thickness variation as shown in Figs. 4(c), (d). That is why analyte's thickness $t_a = 250\,\text{nm}$ was considered while calculating the refractive index sensitivity for plasmonic nanostructures. The increase in the number of higher order waveguide modes was noticed with the increase in the thickness of analyte (Fig. 4(d)), whereas the SP mode and substrate mode were found independent of the thickness variation of the analyte. In Fig. 4(a), we also found the shift in the waveguide mode with variation in refractive index, which is $190\,\text{nm/RIU}$ significantly lower than the sensitivity of SP mode. Since the position of the waveguide mode also shifts with the thickness of analyte of constant refractive index (Figs. 4(c) and (d)), the shift in waveguide modes is not suitable for refractive index sensing. However, the number of these waveguide modes can be used as a coarse method for detecting the thickness of the dielectric superstrate, provided that the refractive index is extracted using the position of the fundamental SP mode at the nanostructure-analyte interface. The occurrence of these higher order waveguide modes has been reported earlier and attributed to the interface of metal and thicker analyte that can support multiple modes, wherein the plasmons with lower momentum propagate with most of the field away from the metal-analyte interface, resulting in lower propagation losses due to weaker interaction with the metal [26].

Since Al-based nanostructures are easy to be oxidized in air, a $3\,\text{nm}$ thin Au layer on the top of Al was considered to avoid the oxidation, as shown in Fig. 5(a), and the transmittivity spectra was calculated again with parameters $t_m = 20\,\text{nm}$ ($17\,\text{nm}$ Al + $3\,\text{nm}$ Au) and $t_g = 20\,\text{nm}$ ($17\,\text{nm}$ Al + $3\,\text{nm}$ Au) for a period (P) of $400\,\text{nm}$, to see the effect on sensing performance as shown in Fig. 5(b). After addition of a $3\,\text{nm}$ thin Au layer, the sensitivity and FWHM were found to be $400\,\text{nm/RIU}$ and $25\,\text{nm}$ respectively which are still decent values from a sensing point of view.

(a)   (b)
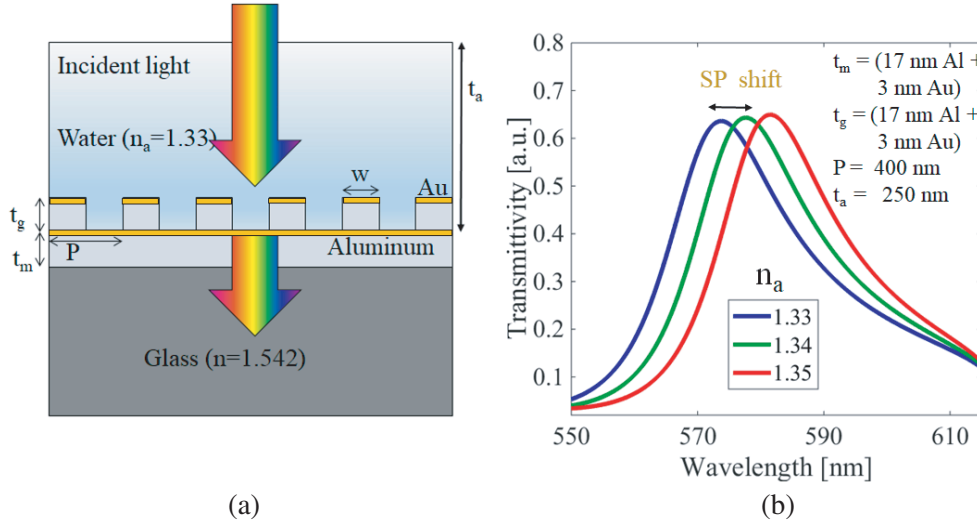
Figure 5. (a) Schematic diagram (not to scale) of the proposed plasmonic nanostructure after addition of $3\,\text{nm}$ Au layer on top of Al. (b) Transmission spectrum for the proposed plasmonic nanostructures of period (P) $= 400\,\text{nm}$, $t_a = 250\,\text{nm}$, $t_m = t_g = 20\,\text{nm}$ ($17\,\text{nm}$ Al + $3\,\text{nm}$ Au) with variation in the refractive index of the analyte.

For enhanced refractive index and thickness sensing applications, we claim that Al-based plasmonic nanostructures may be a better choice than gold based plasmonic nanostructures because of the higher FOM for SPR based sensors and due to the possibility to access the complete UV-VIS-near IR regime for SP based sensing applications. In the case of refractive index estimation of analyte, since the resonance wavelength for excited fundamental SP mode at nanostructure-analyte interface is very sensitive to the change in refractive index, an experiment involving shining a TM polarized broadband light source from the top normal to the surface and collection of the transmitted light from the bottom of the substrate using a high numerical aperture objective may be performed, where the refractive index sensing can be achieved by analyzing the change in the spectral content of the collected light. In the case of the thickness estimation of the analyte, since the number of higher order waveguide modes increases with the increase in the thickness of the analyte, the change in the thickness of the analyte can be observed by capturing the presence of multi-color wavelengths in the spectral content.

3. CONCLUSION

Al-based nanostructures on top of a thin homogenous Al metal coated on a BK-7 glass substrate were engineered in UV-VIS-near IR regime for their sensitivity to an analyte (acting as a superstrate) with different refractive indices and thicknesses. We demonstrated that by carefully choosing a thin homogeneous Al metal layer between a glass substrate and an ultra-low aspect ratio Al-based plasmonic nanostructures, a refractive index sensor with FOM of 22 is possible, which is an improvement by a factor of 4 compared to gold nanostructure-based SPR sensors. The proposed plasmonic nanostructures have potential to be used as refractive index and thickness sensor due to high FOM, high localization of the field, and very low aspect ratio that is needed to maintain laminar flow of analyte and can be used in experiments involving transmission based refractive index and thickness sensors employing normal incidence schemes.

ACKNOWLEDGMENT

REFERENCES

1. Valsecchi, C. and A. G. Brolo, "Periodic metallic nanostructures as plasmonic chemical sensors," *Langmuir*, Vol. 29, No. 19, 5638–5649, 2013.
2. Chung, T., S. Y. Lee, E. Y. Song, H. Chun, and B. Lee, "Plasmonic nanostructures for nano-scale bio-sensing," *Sensors*, Vol. 11, No. 11, 10907–10929, 2011.
3. Špačková, B., P. Wrobel, M. Bocková, and J. Homola, "Optical biosensors based on plasmonic nanostructures: A review," *Proc. IEEE*, Vol. 104, No. 12, 2380–2408, 2016.
4. Arora, P. and A. Krishnan, "Imaging the engineered polarization states of surface plasmon polaritons at visible wavelengths," *J. Light. Technol.*, Vol. 32, No. 24, 4816–4822, 2014.
5. Roh, S., T. Chung, and B. Lee, "Overview of the characteristics of micro- and nano-structured surface plasmon resonance sensors," *Sensors*, Vol. 11, No. 2, 1565–1588, 2011.
6. Homola, J., S. S. Yee, and G. Gauglitz, "Surface plasmon resonance sensors: Review," *Sensors Actuators B Chem.*, Vol. 54, 3–15, 1999.
7. Stewart, M. E., C. R. Anderton, L. B. Thompson, J. Maria, S. K. Gray, J. A. Rogers, and R. G. Nuzzo, "Nanostructured plasmonic sensors," *Chem. Rev.*, Vol. 108, No. 2, 494–521, 2008.
8. González-Campuzano, R., J. M. Saniger, and D. Mendoza, "Plasmonic resonances in hybrid systems of aluminum nanostructured arrays and few-layer graphene within the UV-IR spectral range," *Nanotechnology*, Vol. 28, No. 465704, 1–9, 2017.
9. Lecarme, O., Q. Sun, K. Ueno, and H. Misawa, "Robust and versatile light absorption at near-infrared wavelengths by plasmonic aluminum nanorods," *ACS Photonics*, Vol. 1, No. 6, 538–546, 2014.

10. Su, W., G. Zheng, and X. Li, "Design of a highly sensitive surface plasmon resonance sensor using aluminum-based diffraction gratings," *Opt. Commun.*, Vol. 285, 4603–4607, 2012.

11. Martin, J. and J. Plain, "Fabrication of aluminum nanostructures for plasmonics," *J. Phys. D. Appl. Phys.*, Vol. 48, No. 184002, 1–17, 2015.

12. Li, W., Y. Qiu, L. Zhang, L. Jiang, Z. Zhou, H. Chen, and J. Zhou, "Aluminum nanopyramid array with tunable ultraviolet-visible-infrared wavelength plasmon resonances for rapid detection of carbohydrate antigen 199," *Biosens. Bioelectron.*, Vol. 79, 500–507, 2016.

13. Chowdhury, M. H., K. Ray, S. K. Gray, J. Pond, and J. R. Lakowicz, "Aluminum nanoparticles as substrates for metal-enhanced fluorescence in the ultraviolet for the label-free detection of biomolecules," *Anal. Chem.*, Vol. 81, No. 4, 1397–1403, 2009.

14. Zhang, X., J. Zhao, A. V. Whitney, J. W. Elam, and R. P. Van Duyne, "Ultrastable substrates for surface-enhanced Raman spectroscopy: Al_2O_3 overlayers fabricated by atomic layer deposition yield improved anthrax biomarker detection," *J. Am. Chem. Soc.*, Vol. 128, No. 31, 10304–10309, 2006.

15. Tong, J., F. Suo, J. Ma, L. Y. M. Tobing, L. Qian, and D. H. Zhang, "Surface plasmon enhanced infrared photodetection," *Optoelectron. Adv.*, Vol. 2, No. 1, 1–10, 2019.

16. Lu, H., X. Liu, D. Mao, and G. Wang, "Plasmonic nanosensor based on Fano resonance in waveguide-coupled resonators," *Opt. Lett.*, Vol. 37, No. 18, 3780–3782, 2012.

17. Lu, H., S. Dai, Z. Yue, Y. Fan, H. Cheng, J. Di, D. Mao, E. Li, T. Mei, and J. Zhao, "Sb_2Te_{03} topological insulator: Surface plasmon resonance and application in refractive index monitoring," *Nanoscale*, 2019.

18. Lu, H., Y. Fan, S. Dai, and D. Mao, "Coupling-induced spectral splitting for plasmonic sensing with the ultra-high figure of merit," *Chinese Phys. B*, Vol. 27, No. 11, 117302, 2018.

19. Moharam, M. G., E. B. Grann, and D. A. Pommet, "Formulation for stable and efficient implementation of the rigorous coupled-wave analysis of binary gratings," *J. Opt. Soc. Am. A*, Vol. 12, No. 5, 1068–1076, 1995.

20. Arora, P. and A. Krishnan, "Fourier plane colorimetric sensing using broadband imaging of surface plasmons and application to biosensing," *J. Appl. Phys.*, Vol. 118, No. 23, 2015.

21. Lee, K. L., C. C. Chang, M. L. You, M. Y. Pan, and P. K. Wei, "Enhancing surface sensing sensitivity of metallic nanostructures using blue-shifted surface plasmon mode and fano resonance," *Sci. Rep.*, Vol. 8, No. 1, 1–12, 2018.

22. Arora, P. and A. Krishnan, "On-chip label-free plasmonic-based imaging microscopy for microfluidics," *J. Phys. Commun.*, Vol. 2, No. 085012, 1–9, 2018.

23. Sun, X., X. Shu, and C. Chen, "Grating surface plasmon resonance sensor: Angular sensitivity, metal oxidization effect of Al-based device in optimal structure," *Appl. Opt.*, Vol. 54, No. 6, 1548–1554, 2015.

24. Jha, R. and A. K. Sharma, "High-performance sensor based on surface plasmon resonance with chalcogenide prism and aluminum for detection in infrared," *Opt. Lett.*, Vol. 34, No. 6, 749–751, 2009.

25. Arora, P. and A. Krishnan, "Analysis of transmission characteristics and multiple resonances in plasmonic gratings coated with homogeneous dielectrics," *Progress In Electromagnetics Research Symposium Proceedings*, 927–931, Taipei, March 25–28, 2013.

26. Frisbie, S. P., A. Krishnan, X. Xu, L. G. de Peralta, S. A. Nikishin, M. W. Holtz, and A. A. Bernussi, "Optical reflectivity of asymmetric dielectric-metal-dielectric planar structures," *J. Light. Technol.*, Vol. 27, No. 15, 2964–2969, 2009.